Geophysical Research Letters*

RESEARCH LETTER

10.1029/2022GL100420

Key Points:

- A warming hole appears in a slab ocean model, weaker in absolute magnitude than the observed, but close after removing the global average
- The warming hole is driven by intensified surface westerlies in response to external forcings that lead to cooling via turbulent heat flux
- A novel methodology is developed to identify compensating effects of damping by sea surface temperature and the rise of greenhouse gases

Supporting Information:

Supporting Information may be found in the online version of this article.

Correspondence to:

C. He, cxh1079@rsmas.miami.edu

Citation:

He, C., Clement, A. C., Cane, M. A., Murphy, L. N., Klavans, J. M., & Fenske, T. M. (2022). A North Atlantic warming hole without ocean circulation. *Geophysical Research Letters*, 49, e2022GL100420. https://doi.org/10.1029/2022GL100420

Received 14 JUL 2022 Accepted 20 SEP 2022

A North Atlantic Warming Hole Without Ocean Circulation

Chengfei He¹, Amy C. Clement¹, Mark A. Cane², Lisa N. Murphy¹, Jeremy M. Klavans³, and Tyler M. Fenske¹

¹Rosenstiel School of Marine and Atmospheric Science, University of Miami, Miami, FL, USA, ²Lamont-Doherty Earth Observatory of Columbia University, Palisades, NY, USA, ³Department of Atmospheric and Oceanic Science, University of Colorado Boulder, Boulder, CO, USA

Abstract The sea surface temperature (SST) in the subpolar North Atlantic decreased during the past century, a remarkable feature known as the "warming hole (WH)." It is commonly claimed that the WH results from the slowdown of the Atlantic meridional overturning circulation. However, using an ensemble of the Community Earth System Model coupled to a slab ocean model simulation, we show the atmosphere alone can account for \sim 50% of the observed cooling trend in the subpolar North Atlantic and \sim 90% of the cooling relative to the temperature change of the global ocean. We find this cooling is caused by increased local westerlies in response to external forcing that enhance heat loss from the ocean through turbulent heat fluxes. This cooling is partly compensated by the damping in SST and the warming due to the rise of greenhouse gases. We further suggest that wind-driven ocean processes can enhance the cooling in the real world, but that nonetheless the ultimate driver resides in the atmosphere.

Plain Language Summary The global sea surface temperature (SST) shows a positive trend of ~0.55 K century⁻¹ during the last century (1920–2005), due primarily to the rise in atmospheric CO₂ values. In contrast, the SST in the subpolar North Atlantic has cooled at a rate of ~0.4 K century⁻¹, known as the "warming hole." Many previous studies using climate models link the cooling SST trend to a slowdown of the Atlantic meridional overturning circulation (AMOC), a planetary-scale oceanic circulation transporting heat northward to the high-latitude North Atlantic. However, direct observations linking the cooling SST trend with the slowdown of AMOC remains absent, due to the lack of long-term AMOC observations. Using a climate model without variable ocean currents, we find the atmosphere alone can produce ~50% of the observed cooling trend in the past century. The cooling trend results from the enhanced surface westerly winds that remove heat from ocean surface by enhancing air-sea temperature differences and surface wind strength. This cooling trend is partially compensated by the warming due to the rise of greenhouse gases and the damping effect in SST. We further show that wind-driven ocean processes can enhance the cooling. Our mechanism is consistent with observed changes in the North Atlantic Ocean and atmosphere.

1. Introduction

Since the industrial revolution, the global sea surface temperature (SST) is increasing steadily and rapidly because of anthropogenic fossil-fuel use (IPCC, 2021). However, a pronounced absence of warming, often referred to as the "warming hole (WH)," is observed in the subpolar North Atlantic during the twentieth century. The WH SST is characterized by a cooling trend with an average intensity of ~0.4 K century⁻¹ in 1920–2005 (Figure 1a). This cooling trend has been primarily linked to a weakening of deep convection in the subpolar North Atlantic (Gervais et al., 2018) and, in turn, the slowdown of the Atlantic Meridional Overturning Circulation (AMOC) (Caesar et al., 2018; Latif et al., 2022; Rahmstorf et al., 2015; Sévellec et al., 2017), notably in projected increasing greenhouse gases scenarios (Chemke et al., 2020; Gervais et al., 2018; Keil et al., 2020; Liu et al., 2020; Menary & Wood, 2018; Ren & Liu, 2021).

However, an essential role for AMOC in the past North Atlantic WH remains difficult to establish. First, though a large number of climate models support the slowdown of AMOC causing the WH under global warming (Caesar et al., 2018; Chemke et al., 2020; Gervais et al., 2018; Keil et al., 2020; Liu et al., 2020; Menary & Wood, 2018; Ren & Liu, 2021), the relationship between the centennial North Atlantic cooling and the decline of the AMOC is not established in observations, due primarily to the lack of long-term AMOC measurements (Smeed et al., 2014). Even within the modeling framework, Drijfhout et al. (2012) suggest the appearance of the WH in simulations is earlier than the decline of the AMOC, proposing the potential role of other ocean dynamic

© 2022. American Geophysical Union. All Rights Reserved.

HE ET AL. 1 of 11

from https://agupubs.onlinelibrary.wiley.com/doi/10.1029/2022GL100420 by University Of Mami Libraries, Wiley Online Library on [26/10/2022]. See the 7

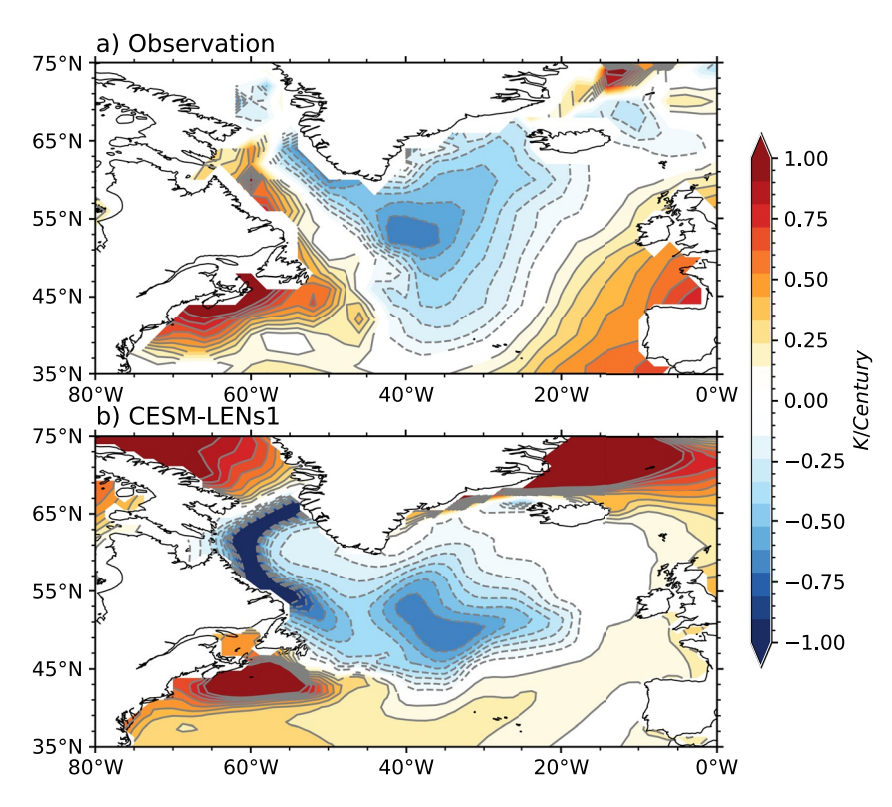


Figure 1. (a) Observed, (b) Community Earth System Model-Large Ensemble Project simulated sea surface temperature (SST) trend during the 1920–2005. The observed SST is derived from an average of the Extended Reconstructed Sea Surface Temperature version 5 and Hadley Centre Sea Ice and Sea Surface Temperature.

processes (e.g., subpolar gyre [Keil et al., 2020] and local deep mixing [Gervais et al., 2018]). Second, the SST is influenced by processes in both the atmosphere and the ocean. In particular, the North Atlantic SST is correlated with climate fluctuations over a wide range of timescales, such as the North Atlantic Oscillation (Clement et al., 2015; Marshall et al., 2001; Simpson et al., 2018). The cooling in SST thus is not exclusively controlled by the AMOC. In addition to the AMOC, recent studies propose that processes, including shortwave cloud feedback, upper layer Ekman heat transports, and storminess over the North Atlantic, could contribute to the formation of WH (Hu & Fedorov, 2020; Keil et al., 2020; Li et al., 2021). In particular, Li et al. (2021) raise an alternative perspective to stress the role of atmospheric forcing in the WH. In an idealized energy balance model driven by observational data, they show the heat loss from the ocean due to increased local storminess overhead can explain ~50% of the observed cooling trend, with the remaining ~50% resulting from mixing layer entrainment. Nevertheless, the role of the atmosphere has not been systemically investigated in a coupled climate model yet, as most studies focus on ocean processes. It remains unclear (a) how the atmospheric circulation can produce a WH by altering surface heat fluxes and (b) whether the WH is driven by internal variability or externally forced, since greenhouse gases, anthropogenic aerosols, and volcanic forcings change significantly in the past century (Klavans et al., 2022).

In our current study, we analyze the impacts of atmospheric circulation and forcings on the WH using an ensemble of slab ocean model (SOM) simulations. The experimental design excludes interactive dynamical ocean circulation and deep mixing and permits us to isolate the ocean influence and to quantify the role of the atmosphere in the WH. The ensemble mean enables us to isolate the role of external forcings in the WH in our model. In our SOM simulation, a WH is simulated in the past century, albeit with a weaker intensity than observations. However, the SOM also has a stronger global warming than is observed, so the difference between the global mean and the WH is only slightly smaller than the observed difference (Table S1 in Supporting Information S1).

Combining reanalysis and our model simulations, we show this WH is a net response of a cooling trend associated with the strengthened air-sea temperature differences and surface wind strength, and a warming trend due to the

HE ET AL. 2 of 11

radiative forcing by greenhouse gases and the passive damping effect in SST. The net effect is primarily driven by the enhanced local westerlies in response to the historical forcings. This paper is organized as follows. In Section 2, we describe the data, model, and methods used in this study. In Section 3, we present our model results and a comparison with observations as well as the fully coupled model, and we also investigate the possibility of a WH driven by internal variability. Section 4 is dedicated to illustrating the mechanism of the WH. Finally, we discuss and conclude our work in Section 5.

2. Data and Methods

2.1. Slab Ocean Model Simulation

A nine-member simulation is conducted using National Center for Atmospheric Research (NCAR) Community Earth System Model 1.1 (CESM1.1, [Hurrell et al., 2013]) with an atmospheric resolution of $0.9^{\circ} \times 1.25^{\circ}$ and an oceanic resolution of $1.125^{\circ} \times 0.27 \sim 0.54^{\circ}$ ($f09_gx1v6$). All 9 members, perturbed at the beginning of each simulation, are forced by the historical forcings spanning from 1920 to 2005, as in the 41-member CESM Large Ensemble Project (CESM-LENs, [Kay et al., 2015]). Unless otherwise stated, our present study uses the ensemble average to investigate the WH, as the ensemble average represents the best estimate of forced historical climate. Readers are encouraged to refer to Murphy et al. (2021) and Text S1 in Supporting Information S1 for detailed model configurations.

2.2. Quantification of the Causes of the Cooling Trend in the North Atlantic

The ocean thermodynamic equation (Equation 1) allows us to calculate the SST offline to quantify the SST trend associated with each individual component of the surface heat flux,

$$\rho c_p h_{\text{mix}} \frac{dT_s}{dt} = (Q_{\text{SW}} + Q_{\text{LW}} + Q_{\text{SH}} + Q_{\text{LH}}) - Q_{\text{flx}} \equiv Q_{\text{sfc}} - Q_{\text{flx}}$$
(1)

where ρ and c_p are the density (=1,026 kg m⁻³) and specific heat capacity (=3,996 J kg⁻¹ K⁻¹) of sea water; h_{mix} is the prescribed mixed layer depth; T_s is the temperature in mixed layer, equivalent to SST; Q_{sfc} the net heat flux into the ocean, is composed of the turbulent heat fluxes, sensible heat (Q_{SH}) and latent heat (Q_{LH}), and the radiative heat fluxes, longwave (Q_{LW}) and shortwave (Q_{SW}). The Q_{flx} in Equation 1 is implemented on the ocean grid (~1 gxIv6) in CESM, but the SST and heat fluxes are output on an atmosphere resolution (0.9° × 1.25°, f09). Remapping Q_{flx} from gxIv6 to f09 would cause a discernible bias in our offline calculation. To avoid this, a linear regression is conducted to derive the Q_{flx} on the atmospheric grid (Appendix A). Then, the contribution of an individual flux to the total SST trend α can be decomposed by:

$$\alpha = \frac{\langle T_s, t \rangle}{\langle t, t \rangle} = \frac{\langle T_s^{\text{SH}}, t \rangle + \langle T_s^{\text{LH}}, t \rangle + \langle T_s^{\text{LW}}, t \rangle + \langle T_s^{\text{SW}}, t \rangle}{\langle t, t \rangle}$$

where subcomponents $(T_s^{SH}, T_s^{LH}, T_s^{LW}, T_s^{SW})$ of T_s are calculated using the monthly mean flux outputs by integrating Equation 1,

$$T_{s}(t) - T_{s}(0) = \frac{1}{\rho c_{p} h_{\text{mix}}} \int_{0}^{t} \overline{Q}_{\text{sfc}} - Q_{\text{flx}} dt + \frac{1}{\rho c_{p} h_{\text{mix}}} \int_{0}^{t} Q'_{\text{sfc}} dt = \frac{1}{\rho c_{p} h_{\text{mix}}} \int_{0}^{t} Q'_{sfc} dt$$

in which $Q'_{\rm sfc}$ is the anomaly from $\overline{Q}_{\rm sfc}$, and $\overline{Q}_{\rm sfc}$ is the average of net surface heat flux over a period (t_s, t_e) where $T_s(t_s) = T_s(t_e)$, which ensures that $\overline{Q}_{\rm sfc} \equiv Q_{\rm flx}$ over this period. Note that this period varies in space, and it is roughly between 1920 and 1940 in the subpolar North Atlantic. By choosing a value for $\overline{Q}_{\rm sfc}$ that makes $\overline{Q}_{\rm sfc} - Q_{\rm flx} = 0$ we ensure that \overline{Q}_{sfc} does only what is needed to give the climatological T_s and does not contribute to SST trends. The trends will then be attributable to $Q'_{\rm sfc} = (Q'_{\rm SW} + Q'_{\rm LW} + Q'_{\rm SH} + Q'_{\rm LH})$, the deviations from the mean quantities.

The intrinsic negative feedbacks in radiative and turbulent heat flux on SST make it difficult to determine the ultimate driving mechanism of the long-term SST trend (Cane et al., 2017). We further decompose the turbulent

HE ET AL. 3 of 11

Table 1				
Linearization of Surface Heat Fluxes	IXES			
Flux	Latent heat	Sensible heat	Longwave	Shortwave
Formula	$Q_{ m LH} = -L ho_a C_E W q_s \left(T_s ight) \left(1 - { m RH} e^{-eta T_s - a} ight)$	$Q_{\rm SH} = -\rho_a C_p C_E W T_{s-a}$	$Q_{\mathrm{LW}} = Q_{\mathrm{LW}}(T_s, T_{s-a}, \mathrm{Cld}, \mathrm{CO}_2, \ldots)$	$Q_{\text{SW}} = Q_{\text{SW}}(\text{Cld}, \dots)$
T_s	$Q_{ m LH}^{o'}=eta \overline{Q}_{ m LH} T_s'$		$Q_{ m LW}^{T_s'}=rac{\partial Q_{ m LW}}{\partial T_s}T_s'$	
W	$Q_{ m LH}^{W'}=\overline{Q}_{ m LH}rac{W'}{\overline{W}}$	$Q_{ m SH}^{W'} = \overline{Q}_{ m SH}^{W'}$		
T_{s-a}	$Q_{\mathrm{LH}}^{T_{s-a}} = \overline{Q}_{\mathrm{LH}} rac{eta \overline{\mathrm{RHe}} - ar{ ho} \overline{T}_{s-a}}{1-\overline{\mathrm{RHe}} - ar{ ho} \overline{T}_{s-a}} T_{s-a}'$	$Q_{ ext{SH}}^{T_{s-a}'} = \overline{Q}_{ ext{SH}} rac{T_{s-a}'}{T_{s-a}}$	$Q_{\mathrm{LW}}^{T'_{s'a}}=rac{\partial Q_{\mathrm{LW}}}{\partial T_{s-a}}T'_{s-a}$	
RH	$Q_{ m LH}^{ m RH'} = -\overline{Q}_{ m LH} rac{e^{-ar{ ho}T_{s-a}}}{1-{ m RH}e^{-ar{ ho}T_{s-a}}}{ m RH'}$			
Cloud			$Q_{ m LW}^{ m Cld'} = rac{\partial Q_{ m LW}}{\partial { m Cl}} { m Cld'}$	$Q_{\rm SW}^{\rm Cld'} = \frac{\partial Q_{\rm SW}}{\partial { m Cld'}} { m Cld'}$
CO ₂			$Q_{\rm LW}^{\rm CO_2'} = \frac{\partial Q_{\rm LW}}{\partial {\rm CO}_2} {\rm CO}_2'$	
Note	$Q_{\rm LH}^{r_{r''}}$ is calculated as a residual in practice	$Q_{ m SH}^{T_{\rm s}^{\prime}-a}$ is calculated as a residual in practice	See main text for linearization of Q_{Lw} by regression	Linearization of $Q_{\rm sw}$ by regression
Note The Table displays the lines	Nate The Table displays the linearization of the surface heat components into subcomponents associated with the deviations from mean values T' W' T' RH' The radiative components also require	popents associated with the deviations fro	m mean values T' W' T' RH' The radiative	components also require

The function $q_s(T)$ is the specific humidity at temperature T following the Clausius-Clapeyron equation. surface relative humidity; β for greenhouse

fluxes into components that can be linked directly to changes in surface wind strength W, SST T_s , surface relative humidity RH, and air-sea temperature differences $T_{s-a} = T_s - T_a$, where T_a is the surface air temperature. For the radiative fluxes we also account for dependence on greenhouse gases ("CO₂") and cloud amount (Cld).

We linearize each component Q about the value \overline{Q} by taking the first terms in a Taylor series:

$$Q' = Q - \overline{Q} \approx \frac{\partial Q}{\partial T_s} T_s' + \frac{\partial Q}{\partial T_{s-a}} T_{s-a}' + \dots + \frac{\partial Q}{\partial \text{Cld}} \text{Cld}' + \frac{\partial Q}{\partial \text{CO}_2} \text{CO}_2'$$

The partial derivatives are evaluated as shown in Table 1. As shown there, we use the standard bulk formulas for $Q_{\rm LH}$ and $Q_{\rm SH}$. Then, as shown in Table 1, Q'_{LH} and Q'_{SH} may be linearized into subcomponents associated with T'_s , W', T'_{s-a} , and RH' using those bulk formulas (Du & Xie, 2008; Xie et al., 2010). For Q_{SW} and Q_{LW} , however, there is not an explicit formula in terms of surface variables to describe the complicated radiative transfer calculation through the atmosphere. For these we estimate the partial derivatives by regressing Q'_{LW} and Q'_{SW} on the T'_s , T'_{s-a} , Cld', ..., and CO'_2 over the whole simulation period. Our calculation shows a set of T'_s , T'_{s-a} , Cld', and CO'_{γ} could explain the Q'_{LW} ($R^2 > 0.95$) and, in turn, the SST and the Q'_{SW} could be explained by the Cld' over the North Atlantic (Table 1). In this decomposition of radiative fluxes, we do not explicitly include a term for anthropogenic aerosols because they are highly collinear with CO₂ (particularly before 1980; Deser et al., 2020). As such, coefficients associated with CO₂ may also capture some of the response to global and/or regional anthropogenic aerosols. We also calculated the decomposition to Q'_{LH} and Q'_{SH} by regression and the results are very close to the decomposition based on the bulk formulas (not shown).

Table 1 summarizes the decomposition in the present study. The first row is the decomposition of SST trend associated with individual heat fluxes, and the first column shows the decomposition associated with the physical factors. In short, we identify five driving factors in the atmosphere including W, T_{s-a} , RH, Cld, and CO_2 (as well as anthropogenic aerosols) and one damping effect due to T_s .

2.3. Observational and Modeled Data

Observed SST cooling trend is calculated based on the compiled National Oceanic and Atmospheric Administration (NOAA) Extended Reconstructed Sea Surface Temperature version 5 (ERSSTv5) (Huang et al., 2017) and Met Office Hadley Centre Sea Ice and Sea Surface Temperature (HadISST) (Rayner et al., 2003). For consistency, SSTs from 1920 to 2005 are selected and interpolated to $2^{\circ} \times 2^{\circ}$ grid. In addition, atmospheric data including air temperature (2 m), surface temperature, surface and high level (500 hPa) winds, and total cloud cover are taken from National Centers for Environmental Prediction reanalysis (NCEP, 1949–2005) (Kalnay et al., 1996) and Coupled reanalysis of the twentieth Century (CERA-20C) from the European Centre for Medium-Range Weather Forecasts (ECMWF, 1920–2005) (Laloyaux et al., 2018), respectively. The CERA-20C is a 10-member ensemble of coupled climate reanalysis, and the ensemble average is used in present study. Corresponding CESM-LENs data (Kay et al., 2015) are also used to compare the SST trend in the North Atlantic.

19448007, 2022, 19, Downloaded

from https://agupubs.onlinelibrary.wiley.com/doi/10.1029/2022GL100420 by University Of Miami Libraries, Wiley Online Library on [26/10/2022]. See the Terms and Cond

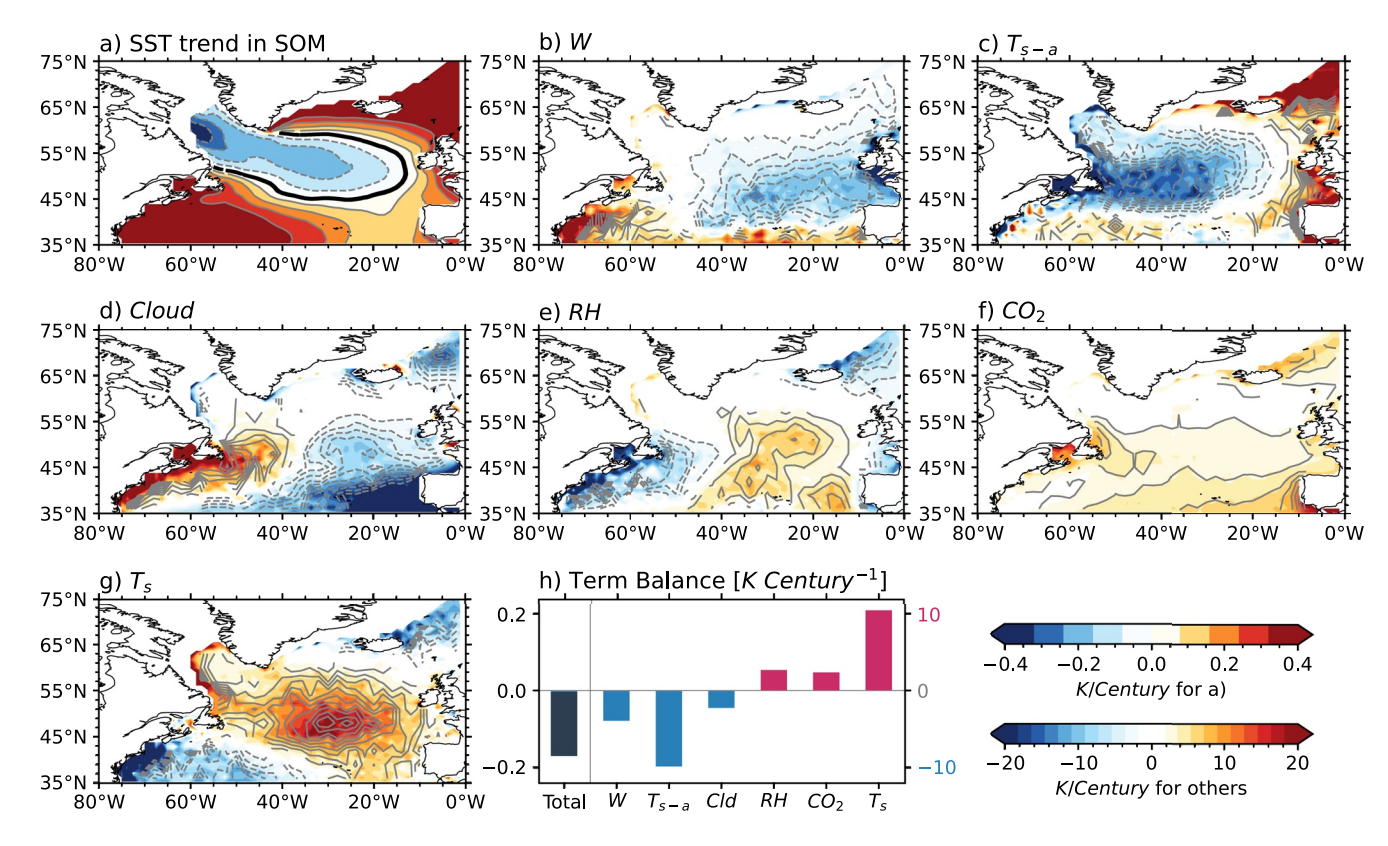


Figure 2. (a) Slab ocean model simulated North Atlantic sea surface temperature (SST) trend (shading and contour) during the 1920–2005 and its subcomponents due to changes in: (b) surface wind strength, (c) air-sea temperature difference, (d) low-level cloud covers, (e) relative humidity, (f) greenhouse gases, and (g) SST. (h) Contributions of each term in the warming hole region where SST has a cooling trend. The "Total" corresponds to the left *y*-axis and others are on the right *y*-axis. In (a), the zero-contour is outlined as bold black.

3. Observed and Simulated WH

The observed and CESM-LENs cooling trends are shown in Figure 1. The observed cooling at a rate of \sim 0.4 K Century⁻¹ is primarily located in the subpolar North Atlantic and extends northward to the Irminger and Labrador Seas (Figure 1a). The ensemble average SST in the fully coupled CESM-LENs is similar to the observed trend in the subpolar North Atlantic, with the notable exception of a cooling maximum that appears in the Labrador Sea (Figure 1b), which has been previously explained by Gervais et al. (2018) as a suppression of deep convection. A cooling trend is also present in the SOM simulation (Figure 2a). Resembling the fully coupled model, the cooling SST in SOM extends from the Labrador Sea to the interior North Atlantic, but the maximum cooling in the subpolar North Atlantic is muted.

The time series of the WH index is portrayed in Figure S1a in Supporting Information S1. The index is defined as the difference of WH SST from the global ocean average. The WH indices in observations and the SOM are characterized by strong interannual-to-multidecadal variability, with a cooling trend between the 1930s and 1990s and a warming afterward. Against the SOM, the WH index in CESM-LENs is manifested as a monotonic cooling before 1960, a slight warming and a cooling delineated by 1985. The multidecadal variability in the fully coupled CESM-LENs is strongly damped by ocean dynamics (Murphy et al., 2021). The WH SST is similar to the WH index (Figure S1b in Supporting Information S1). Overall, the WH cooling in SOM is around 50% of the CESM-LENs, but the former global warming is also 50% higher than the later (Table S1 in Supporting Information S1), because of the fixed mixed layer depth and the absence of vertical mixing in CESM-SOM. As such, relative to the global average, the WH intensity is similar in CESM-SOM and CESM-LENs, and both are slightly smaller than the observed difference (Table S1 in Supporting Information S1). This also remains similar, if we define the WH cooling as the SST differences between the cooling region and the rest of subpolar North Atlantic (as in Hu & Fedorov, 2020).

HE ET AL. 5 of 11

The North Atlantic SST is argued to be driven by the internal atmospheric or oceanic dynamics, including the AMOC and NAO (Clement et al., 2015; Zhang et al., 2019). To quantify the possibility of an internally driven WH, we randomly choose 86-year long SST time series (same as the length of historical period: 1920–2005) from an 1000-year SOM pi-control simulation, and calculate the trend of the WH index as well as its correlation with the observations. This process is repeated for 1000 times. The joint distribution of the correlations and trends is shown in Figure S1c in Supporting Information S1, which shows the ensemble mean of the historical SOM simulation stands outside of the cluster. This implies a largely forced historical WH in both the trend and the multidecadal variability. Similar results hold, if we calculate the correlation between North Atlantic SST and observations (Figure S1d in Supporting Information S1). Nevertheless, given the observed SST has strong interannual-to-multidecadal variability (Figure S1b in Supporting Information S1), the internal variability may affect the SST in the WH region. In this study, we focus on the forced response.

4. WH Driven by the Westerlies

To examine the mechanism of the cooling in the CESM-SOM, we first quantify the SST trend associated with individual surface heat flux (Table 1, first row). At face value, this cooling trend is led by $Q_{\rm SH}$, while $Q_{\rm LH}$ and $Q_{\rm LW}$ produce a significant warming that offsets the $Q_{\rm SW}$ cooling (Figure S2a in Supporting Information S1). Spatially, the $Q_{\rm SW}$ gives rise to a west-east dipole SST response in the North Atlantic, with a prominent cooling trend in the eastern basin and warming trend in the western basin. This dipole trend, however, is largely compensated by the opposite trends due to $Q_{\rm LW}$ and $Q_{\rm LH}$. The compensation between $Q_{\rm SW}$ and $Q_{\rm LW}$ is not surprising, but why is the SST trend associated with $Q_{\rm SH}$ not consistent with the $Q_{\rm LH}$ trend, since their driving components (winds, SST) have a high degree of similarity? Or equivalently, what are the driving mechanisms of SST trend in the turbulent fluxes and ultimately the WH in the SOM?

The net SST trend in the WH is driven by the cooling associated with surface wind strength and air-sea temperature differences across the North Atlantic basin (Figure 2h; Table 1, first column). The wind strength induced cooling peaks in the eastern basin, decays toward to the interior North Atlantic, and even reverses in the Gulf Stream (Figure 2b). In contrast, the air-sea temperature differences induced cooling is largest in the western basin, stretching to the mid subpolar North Atlantic (Figure 2c). The cooling trends are strongly compensated by the damping effect from the SST (Figure 2h), which on its own induces a warming tendency in most of the North Atlantic (Figure 2g). Greenhouse gases on their own produce a warming throughout the basin, as expected (Figure 2f). The SST trends associated with relative humidity and low-level cloud cover display a west-east dipole response, and are largely opposite (Figure 2d, 2e and 2h).

The cooling trend associated with surface wind strength and air-sea temperature difference stems from an increase in the surface westerlies during the last century. Figure 3a shows the simulated trend of surface wind strength, the pattern of which is consistent with the cooling in Figure 2b. The enhancement of boundary-layer wind speed is mainly manifested by the poleward shift in the westerly winds, a robust response in agreement with the reanalysis (Figures 3a and 3b; Figure S3a in Supporting Information S1) and a number of previous studies (Chang & Yau, 2016; Feser et al., 2015; Woollings et al., 2012). Physically, an increase in wind speed would amplify Q_{SH} and Q_{LH} to extract energy out of the ocean, leading to a cooling effect (Figure S2c in Supporting Information S1).

The increase in surface westerlies also enhances the air-sea temperature differences. Figure 3c shows the air-sea temperature difference in SOM is well correlated with the temperature advection, which is mostly due to the surface westerlies across the WH regions (Figure S4a in Supporting Information S1). The intensified surface wind transports more cold air from the nearby North American continent and high latitudes to the North Atlantic, such that the boundary air over the ocean is cooler than the ocean water (Seager et al., 1995). Consequently, the air-sea temperature differences increase; the associated Q_{SH} and Q_{LH} increase, producing the cooling SST trend.

A role for surface westerlies in the air-sea temperature differences is also observed in NCEP and CERA-20C reanalyses (Figure 3d, and Figures S4b–S4d in Supporting Information S1). Both SOM and reanalysis data show highest correlations in the Labrador Sea that stretches to the interior subpolar North Atlantic. Due to the increase in the surface westerly winds (Figure 3b), a cooling trend associated with air-sea temperature differences in observations is also expected as in the SOM. Interestingly, the pattern of WH resembles the correlation map in reanalysis

HE ET AL. 6 of 11

19448007, 2022, 19, Downloaded from https://agupubs.onlinelibrary.wiley.com/doi/10.1029/2022GL100420 by University Of Mfami Libraries, Wiley Online Library on [26/10/2022]. See the Terms and Conditions (https://onlinelibrary.wiley

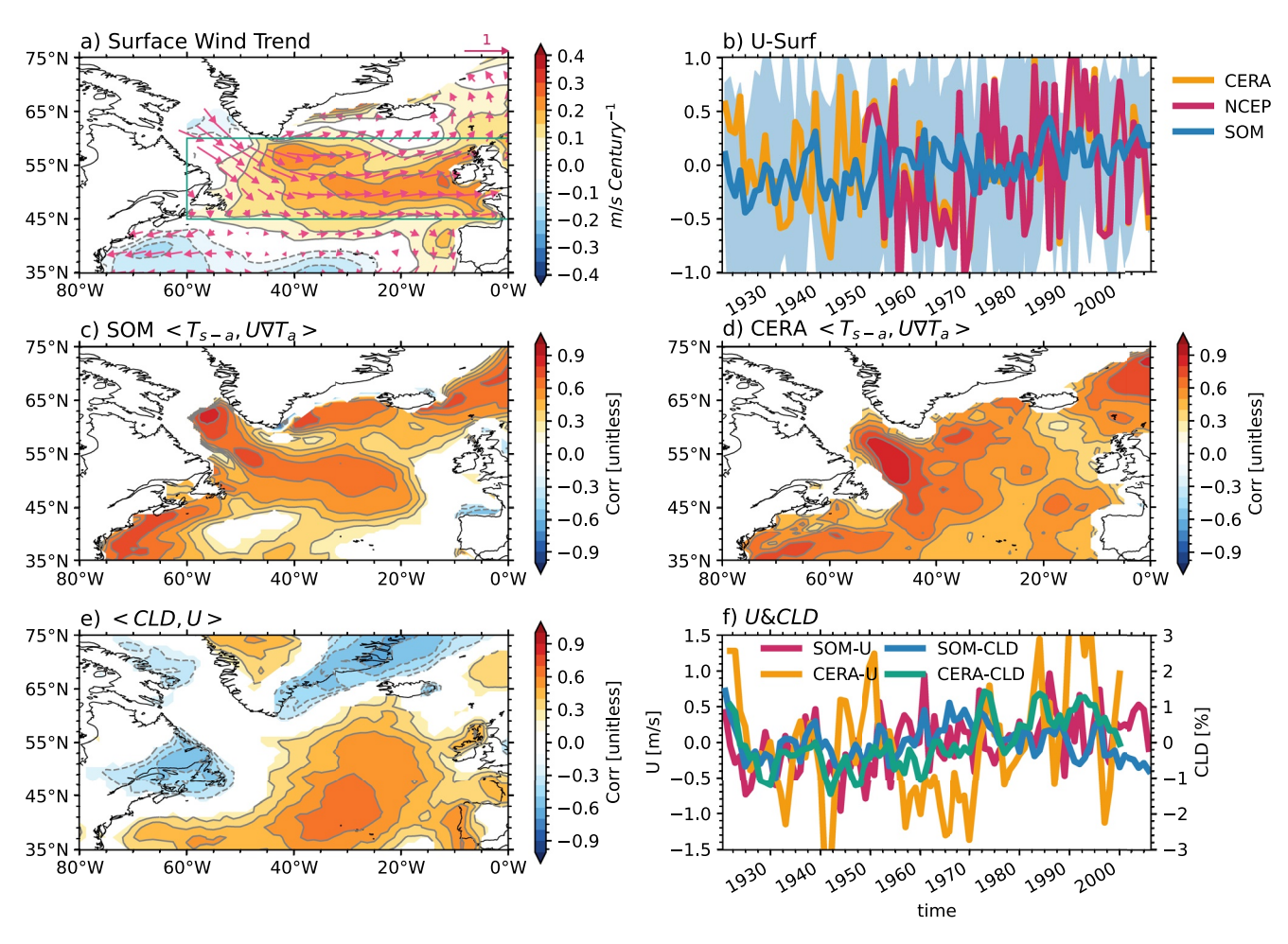


Figure 3. (a) Slab ocean model (SOM) simulated North Atlantic surface wind speed (shading) and wind (vector) trend during the 1920–2005, (b) Timeseries of averaged subpolar North Atlantic surface westerly in SOM and reanalysis, (c) Correlation between air-sea temperature difference and surface temperature advection in SOM, (d) as in (c) but for CREA-20C reanalysis, (e) Correlation between cloud coverage and high-level westerly in SOM, (f) Timeseries of averaged subpolar North Atlantic high-level westerly (left-axis) and cloud coverage (right-axis) in SOM and reanalysis (see legend). In (b), the light blue envelope is ensemble spread in SOM. the subpolar North Atlantic is defined as 45°–60°N, 60°–0°W, which is marked as green box in (a). In (c–e), correlations at 95% (p < 0.05) confidence level in two-tailed Student's t-test are plotted. In (f), a 3-year running mean is applied to CREA-20C reanalysis for visualization. The westerly from reanalysis is on 500 hPa, while that in SOM is averaged between 400 and 700 hPa on native hybrid-pressure model level, which is close to 500 hPa. Climatology has been removed in all timeseries for comparison.

and SOM, respectively (Figures 1a vs. 3d and Figure S4b in Supporting Information S1; Figures 2a vs. 3c and Figure S4a in Supporting Information S1), demonstrating the role of surface westerlies in creating the WH.

The dipole SST trend from cloud coverage also arises from a change in the high-altitude westerlies, which shows the jet core shifts poleward and elongates eastward over the last century (Figure S3a in Supporting Information S1) (Gervais et al., 2019). As a result, the low-level cloud cover increases in the eastern basin and decreases in the west (Figure S3b in Supporting Information S1), which leads to an opposing SST response in Q_{SW} and Q_{LW} (Figure S2f in Supporting Information S1). Overall, Q_{SW} dominates the net response. Again, the relationship between cloudiness and the westerly jet stream is examined in the reanalysis, and NCEP and CERA-20C show similar results to the SOM simulation (Figure 3f and Figure S5 in Supporting Information S1). This relationship is consistent with previous studies (Bender et al., 2012; Li et al., 2021).

However, the dipole SST pattern generated from cloud is largely canceled by that from the relative humidity. In response to the shift of westerlies and cloudiness, the near-surface relative humidity also increases in the east basin and decreases in the west (Figure S3c in Supporting Information S1), thus triggering an opposite SST trend via Q_{LH} (Figure 2e and Figure S2e in Supporting Information S1).

HE ET AL. 7 of 11

wiley.com/doi/10.1029/2022GL100420 by University Of Miami Libraries,

Wiley Online Library on [26/10/2022].

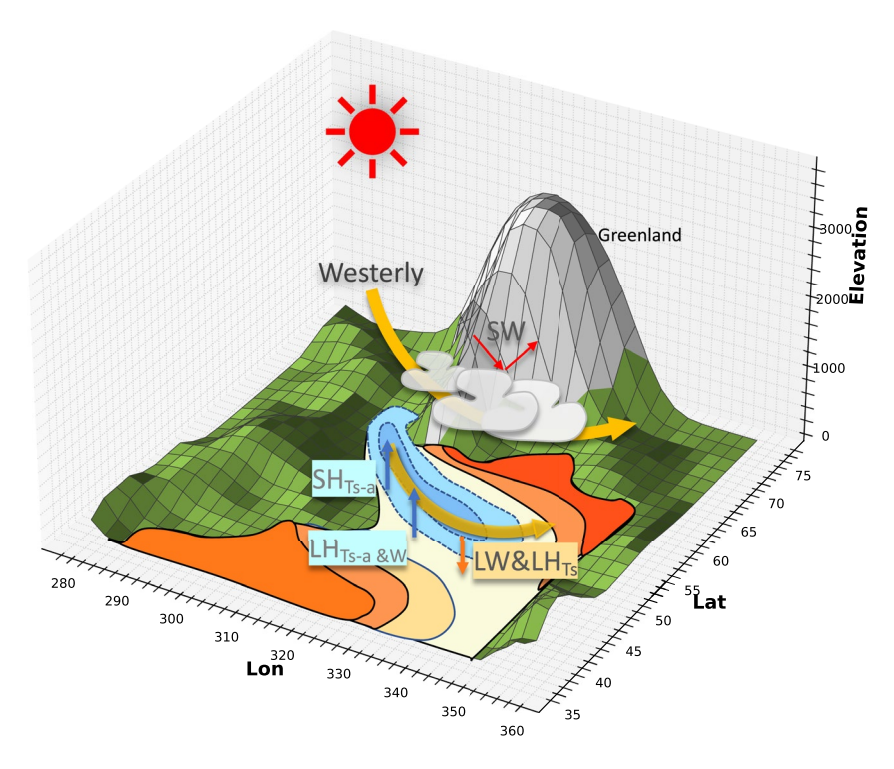


Figure 4. Schematic plot for the mechanism of warming hole in the North Atlantic.

Finally, the cooling driven by surface wind speed and air-sea temperature differences is heavily offset by the damping from SST associated with Q_{LH} and the warming from greenhouse gases associated with Q_{LW} (Figure 2; Figures S2b and S2g in Supporting Information S1). The SST damping effect is expected. As the surface wind strength and air-sea temperature differences cool the SST, the dependence of Q_{LH} and upward Q_{LW} on SST warms the SST up by reducing the outgoing Q_{LH} and Q_{LW} (i.e., a negative feedback). This damping is largely accomplished by Q_{LH} (Figure S2b in Supporting Information S1), rather than by Q_{LW} , because the upward Q_{LW} (T_s') is nearly perfectly compensated by the downward Q_{LW} (T_a'), leaving a small net cooling response in the Q_{LW} (T_{s-a}') (Figure S2d4 in Supporting Information S1). Instead, the rise in CO_2 causes a warming SST trend in Q_{LW} , weakening the cooling from W' and T_{s-a}' (Figure S2g in Supporting Information S1). Spatial deviations from a uniform CO_2 warming - in particular the weak warming in the subpolar gyre—may result from the background ocean state (Marshall et al., 2014), local climate feedbacks (Soden et al., 2008), as well as uneven anthropogenic aerosol emissions (Deser et al., 2020) that coevolves with the CO_2 before 1980 (Text S2 in Supporting Information S1). Note that though the CO_2 causes a warming SST trend directly, it also shifts the westerlies (Chang & Yau, 2016; Feser et al., 2015; Li et al., 2021; Woollings et al., 2012) and causes a cooling trend indirectly.

5. Conclusion and Discussion

5.1. Concluding Remarks

We conclude that a forced North Atlantic WH is simulated in an ensemble of SOM simulations that lack an active ocean, which could explain about 50% of the cooling in observation in the past century, or almost 90% of the difference between the WH and the global mean trends. The detailed mechanism of the WH associated with the westerlies is summarized in Figure 4. The westerlies shift poleward as a response to historical forcings during the past century and influences the radiative and turbulent heat fluxes. At the surface, the intensified wind strength amplifies air-sea temperature differences, and both drive an oceanic heat loss through latent and sensible heat fluxes. In the atmosphere, the correlated shift of clouds blocks the shortwave radiation but increases downward longwave radiation to the North Atlantic, the net effect of which is, however, largely balanced by the relative humidity change near the surface. Though the cooling induced by winds and air-sea temperature differences is strongly offset by the SST feedback and by the warming due to greenhouse gases, the WH persists in the subpolar

HE ET AL. 8 of 11

5.2. Comparing SOM With Observation and CESM-LENs

Though our SOM simulation and CESM-LENs both produce a WH in the North Atlantic, the cooling pattern has some differences with observations. In particular, the cooling maximum in the Labrador Sea in models is absent in observations. In our SOM simulations, this cooling peak originates from temperature advection by the surface westerlies. The air-sea temperature difference and surface westerlies show tightest coherence in the Labrador Sea, as the sea surface starts to be exposed to the open air at the edge of sea ice and thus the SST is mostly impacted by the cold air advected by the surface wind. This cooling maximum is amplified in the CESM-LENs, probably by the suppression of deep convection (Gervais et al., 2018).

The last notable difference is that the WH in SOM is northward displaced compared to the observation, which may be due to the absence of oceanic Ekman heat transport. Figure S6a in Supporting Information S1 plots the trend of Ekman heat transport in SOM, in which a swath of heat divergence (~3 W m⁻² Century⁻¹) region is located at around 50°N in the subpolar North Atlantic. This cooling effect is attributable to advection of mean SST gradients by anomalous wind stress (Figure S6b in Supporting Information S1) (Hu & Fedorov, 2020). With an Ekman flow included in SOM, the WH would shift southward and have a cooling maximum in the subpolar North Atlantic. It is noted that the anomalous Ekman heat transport here is calculated offline. Developing an Ekman flow and deep mixing explicitly resolved SOM (Hsu et al., 2022) would further our understanding of the oceanic processes that contribute to the WH. In addition to the anomalous Ekman heat transport, the cooling ocean surface could weaken the local ocean stratification and increase the frequency of convection that would produce an additional cooling effect (Li et al., 2021).

Nonetheless, our model results, combined with reanalysis, suggest that atmospheric circulation changes can produce cooling not only through surface fluxes, but also by driving anomalous Ekman heat transports in the ocean, which together may explain widespread cooling of the North Atlantic in historical observations, without a role for the AMOC. Indeed, the multi-model simulated AMOC shows an overall increasing trend in the past century in the Coupled Model Intercomparison Project 6 (Hassen et al., 2021; Menary et al., 2020), further stressing the important role of the atmosphere in the WH. In future warming scenarios, our preliminary results (not shown) and other peer studies (Keil et al., 2020), however, suggest that the absolute cooling trend in SOM disappears from the North Atlantic but the WH persists in fully coupled models, suggesting the dominating role of oceanic processes in the future (Chemke et al., 2020; Gervais et al., 2018; Keil et al., 2020; Liu et al., 2020; Menary & Wood, 2018; Ren & Liu, 2021) due to the heat uptake in the North Atlantic (He et al., 2019; Ma et al., 2020).

5.3. Fingerprint of the AMOC

The fingerprint of cooling in the subpolar Atlantic Ocean and warming in the Gulf Stream has been used as a proxy for the AMOC strength (Caesar et al., 2018; Rahmstorf et al., 2015). This fingerprint along with the warming in the South Atlantic also emerges in our SOM simulations purely driven by the atmospheric dynamics and is similar to the observation (Figure S7 in Supporting Information S1 vs. Figure 2 in Caesar et al., 2018). Given that SST is heavily influenced by atmospheric processes, this raises concerns about inferring the state of the AMOC based on SST. Subsurface temperature is a better alternate (He et al., 2020; Zhang, 2008).

Appendix A: Derive the Q_{flx} on f09 Grid

To calculate the SST associated with individual heat flux, we have to first derive the Q_{flx} on atmospheric grid (f09). Integrating Equation 1 on both sides, it is easy to have

$$T(t) - T(0) - \frac{1}{\rho c_p h_{\text{mix}}} \int_0^t Q_{\text{sfc}} dt = \frac{1}{\rho c_p h_{\text{mix}}} Q_{\text{flx}} t$$
(A1)

HE ET AL. 9 of 11

19448007, 2022,

T(t) and Q_{sfc} are available on the left hand side. Since Q_{flx} is a constant at each grid, the right hand side of Equation A1 $\frac{1}{\rho c_n h_{\text{mix}}} Q_{\text{flx}}$ is just the regression coefficient giving the best least squares fit.

Data Availability Statement

ERSST v5 is publicly at: https://psl.noaa.gov/data/gridded/data.noaa.ersst.v5.html. HadISST is publicly at: https://www.metoffice.gov.uk/hadobs/hadisst/. NCEP/NCAR Reanalysis 1 is available at: https://psl.noaa.gov/data/%20gridded/data.ncep.reanalysis.html. The CERA-20C renanlysis is available at: https://www.ecmwf.int/en/forecasts/dataset/coupled-reanalysis-20th-century. The CESM-LENs data is available at: https://www.cesm.ucar.edu/projects/community-projects/LENS/. The SOM data and the data supporting the findings of this study are available at: https://doi.org/10.5281/zenodo.6835371.

Acknowledgments

The authors would acknowledge support for this work from NOAA Grant NA20OAR4310400, NSF Climate and Large-Scale Dynamics Grants AGS 1735245 and from NSF P2C2 Grant AGS 1735245 and from NSF P2C2 Grant AGS 1703076. We would like to thank Sarah Larson for discussions about the Ekman transports. We would like to thank two anonymous reviewers for their constructive comments. The authors would like to acknowledge high-performance computing support from Cheyenne (https://doi.org/10.5065/D6RX99HX) carried on NCAR's Computational and Information Systems Laboratory.

References

- Bender, F. A.-M., Ramanathan, V., & Tselioudis, G. (2012). Changes in extratropical storm track cloudiness 1983–2008: Observational support for a poleward shift. Climate Dynamics, 38(9–10), 2037–2053. https://doi.org/10.1007/s00382-011-1065-6
- Caesar, L., Rahmstorf, S., Robinson, A., Feulner, G., & Saba, V. (2018). Observed fingerprint of a weakening Atlantic Ocean overturning circulation. *Nature*, 556(7700), 191–196. https://doi.org/10.1038/s41586-018-0006-5
- Cane, M. A., Clement, A. C., Murphy, L. N., & Bellomo, K. (2017). Low-pass filtering, heat flux, and Atlantic multidecadal variability. *Journal of Climate*, 30(18), 7529–7553. https://doi.org/10.1175/jcli-d-16-0810.1
- Chang, E. K. M., & Yau, A. M. W. (2016). Northern Hemisphere winter storm track trends since 1959 derived from multiple reanalysis datasets. Climate Dynamics, 47(5), 1435–1454. https://doi.org/10.1007/s00382-015-2911-8
- Chemke, R., Zanna, L., & Polvani, L. M. (2020). Identifying a human signal in the North Atlantic warming hole. *Nature Communications*, 11(1), 1540. https://doi.org/10.1038/s41467-020-15285-x
- Clement, A., Bellomo, K., Murphy, L. N., Cane, M. A., Mauritsen, T., Radel, G., & Stevens, B. (2015). The Atlantic Multidecadal Oscillation without a role for ocean circulation. *Science*, 350(6258), 320–324. https://doi.org/10.1126/science.aab3980
- Deser, C., Phillips, A. S., Simpson, I. R., Rosenbloom, N., Coleman, D., Lehner, F., et al. (2020). Isolating the evolving contributions of anthropogenic aerosols and greenhouse gases: A new CESM1 large ensemble community resource. *Journal of Climate*, 33(18), 7835–7858. https://doi.org/10.1175/jcli-d-20-0123.1
- Drijfhout, S., van Oldenborgh, G. J., & Cimatoribus, A. (2012). Is a decline of AMOC causing the warming hole above the North Atlantic in observed and modeled warming patterns? *Journal of Climate*, 25(24), 8373–8379. https://doi.org/10.1175/JCLI-D-12-00490.1
- Du, Y., & Xie, S.-P. (2008). Role of atmospheric adjustments in the tropical Indian Ocean warming during the 20th century in climate models. Geophysical Research Letters, 35(8), L08712. https://doi.org/10.1029/2008g1033631
- Feser, F., Barcikowska, M., Krueger, O., Schenk, F., Weisse, R., & Xia, L. (2015). Storminess over the North Atlantic and northwestern Europe—A review. *Quarterly Journal of the Royal Meteorological Society*, 141(687), 350–382. https://doi.org/10.1002/qj.2364
- Gervais, M., Shaman, J., & Kushnir, Y. (2018). Mechanisms governing the development of the North Atlantic warming hole in the CESM-LE future climate simulations. *Journal of Climate*, 31(15), 5927–5946. https://doi.org/10.1175/jcli-d-17-0635.1
- Gervais, M., Shaman, J., & Kushnir, Y. (2019). Impacts of the North Atlantic warming hole in future climate Projections: Mean atmospheric circulation and the North Atlantic jet. *Journal of Climate*, 32(10), 2673–2689. https://doi.org/10.1175/jcli-d-18-0647.1
- Hassan, T., Allen, R. J., Liu, W., & Randles, C. A. (2021). Anthropogenic aerosol forcing of the Atlantic meridional overturning circulation and the associated mechanisms in CMIP6 models. *Atmospheric Chemistry and Physics*, 21(8), 5821–5846. https://doi.org/10.5194/acp-21-5821-2021
- He, C., Liu, Z., & Hu, A. (2019). The transient response of atmospheric and oceanic heat transports to anthropogenic warming. *Nature Climate Change*, 9(3), 222–226. https://doi.org/10.1038/s41558-018-0387-3
- He, C., Liu, Z., Zhu, J., Zhang, J., Gu, S., Otto-Bliesner, B. L., et al. (2020). North Atlantic subsurface temperature response controlled by effective freshwater input in "Heinrich" events. Earth and Planetary Science Letters, 539, 116247. https://doi.org/10.1016/j.epsl.2020.116247 Hsu, T.-Y., Primeau, F., & Magnusdittirm, &G. (2022). A hierarchy of global ocean models coupled to CESM1. Journal of Advances in Modeling
- Earth Systems, 14(8). https://doi.org/10.1029/2021MS002979

 Hu, S., & Fedorov, A. V. (2020). Indian Ocean warming as a driver of the North Atlantic warming hole. Nature Communications, 11(1), 4785. https://doi.org/10.1038/s41467-020-18522-5
- Huang, B., Thorne, P. W., Banzon, V. F., Boyer, T., Chepurin, G., Lawrimore, J. H., et al. (2017). Extended reconstructed sea surface temperature, Version 5 (ERSSTv5): Upgrades, validations, and intercomparisons. *Journal of Climate*, 30(20), 179–8205. https://doi.org/10.1175/JCI.I-D-16-0836.1
- Hurrell, J. W., Holland, M. M., Gent, P. R., Ghan, S., Kay, J. E., Kushner, P. J., et al. (2013). The community Earth system model: A framework for collaborative research. *Bulletin of the American Meteorological Society*, 94(9), 339–1360. https://doi.org/10.1175/BAMS-D-12-00121.1
- IPCC. (2021). Climate change 2021: The physical science basis. Contribution of working Group I to the sixth Assessment report of the intergovernmental Panel on climate change [Masson-Delmotte, Zhai, P., Pirani, A., et al. (eds.)]. In The NCEP/NCAR 40-year reanalysis project (pp. 437–471). Bulletin of the American Meteorological Society. https://doi.org/10.1175/1520-0477(1996)077<0437:TNYRP>2.0.CO;2
- Kalnay, E., Kanamitsu, M., Kistler, R., Collins, W., Deaven, D., Gandin, L., et al. (1996). The NCEP/NCAR 40-year reanalysis project. *Bulletin of the American Meteorological Society*, 77(3), 437–471. https://doi.org/10.1175/1520-0477(1996)077<0437:TNYRP>2.0.CO;2
- Kay, J. E., Deser, C., Phillips, A., Mai, A., Hannay, C., Strand, G., et al. (2015). The community Earth system model (CESM) large ensemble project: A community resource for studying climate change in the presence of internal climate variability. *Bulletin of the American Meteorological Society*, 96(8), 1333–1349. https://doi.org/10.1175/BAMS-D-13-00255.1
- Keil, P., Mauritsen, T., Jungclaus, J., Hedemann, C., Olonscheck, D., & Ghosh, R. (2020). Multiple drivers of the North Atlantic warming hole. Nature Climate Change, 10(7), 667–671. https://doi.org/10.1038/s41558-020-0819-8
- Klavans, J. M., Clement, A. C., Cane, M. A., Murphy, L. N., & Cane, M. A. (2022). The evolving role of external forcing in North Atlantic SST variability over the last Millennium. *Journal of Climate*, 35(9), 2741–2754. https://doi.org/10.1175/JCLI-D-21-0338.1

HE ET AL. 10 of 11

- Laloyaux, P., de Boisseson, E., Balmaseda, M., Bidlot, J.-R., Broennimann, S., Buizza, R., et al. (2018). CERA-20C: A coupled reanalysis of the twentieth century. *Journal of Advances in Modeling Earth Systems*, 10(5), 1172–1195. https://doi.org/10.1029/2018ms001273
- Latif, M., Sun, J., Visbeck, M., & Hadi Bordbar, M. (2022). Natural variability has dominated Atlantic meridional overturning circulation since 1900. Nature Climate Change, 12(5), 455–460. https://doi.org/10.1038/s41558-022-01342-4
- Li, L., Lozier, M. S., & Li, F. (2021). Century-long cooling trend in subpolar North Atlantic forced by atmosphere: An alternative explanation. Climate Dynamics, 58(9–10), 2249–2267. https://doi.org/10.1007/s00382-021-06003-4
- Liu, W., Fedorov, A. V., Xie, S.-P., & Hu, S. (2020). Climate impacts of a weakened Atlantic meridional overturning circulation in a warming climate. Science Advances, 6(26), eaaz4876. https://doi.org/10.1126/sciadv.aaz4876
- Ma, X., Liu, W., Allen, R. J., Huang, G., & Li, X. (2020). Dependence of regional ocean heat uptake on anthropogenic warming scenarios. *Science Advances*, 6(45). https://doi.org/10.1126/sciadv.abc0303
- Marshall, J., Armour, K. C., Scott, J. R., Kostov, Y., Hausmann, U., Ferreira, D., et al. (2014). The ocean's role in polar climate change: Asymmetric Arctic and Antarctic responses to greenhouse gas and ozone forcing. *Philosophical Transactions of the Royal Society A: Mathematical, Physical & Engineering Sciences*, 372, 20130040. https://doi.org/10.1098/rsta.2013.0040
- Marshall, J., Kushnir, Y., Battisti, D., Chang, P., Czaja, A., Dickson, R., et al. (2001). North Atlantic climate variability: Phenomena, impacts and mechanisms. *International Journal of Climatology: A Journal of the Royal Meteorological Society*, 21(15), 1863–1898. https://doi.org/10.1002/joc.693
- Menary, M. B., & Wood, R. A. (2018). An anatomy of the projected North Atlantic warming hole in CMIP5 models. Climate Dynamics, 50(7–8), 3063–3080. https://doi.org/10.1007/s00382-017-3793-8
- Menary, M. B., Robson, J., Allan, R. P., Booth, B. B. B., Cassou, C., Gastineau, G., et al. (2020). Aerosol-forced AMOC changes in CMIP6 historical simulations. Geophysical Research Letters, 47(14), e2020GL088166. https://doi.org/10.1029/2020gl088166
- Murphy, L. N., Klavans, J. M., Clement, A. C., & Cane, M. A. (2021). Investigating the roles of external forcing and ocean circulation on the Atlantic multidecadal SST variability in a large ensemble climate model hierarchy. *Journal of Climate*, 1–51. https://doi.org/10.1175/icli-d-20-0167.1
- Rahmstorf, S., Box, J. E., Feulner, G., Mann, M. E., Robinson, A., Rutherford, S., & Schaffernicht, E. J. (2015). Exceptional twentieth-century slowdown in Atlantic Ocean overturning circulation. *Nature Climate Change*, 5(5), 475–480. https://doi.org/10.1038/nclimate2554
- Rayner, N. A. A., Parker, D. E., Horton, E. B., Folland, C. K., Alexander, L. V., Rowell, D. P., et al. (2003). Global analyses of sea surface temperature, sea ice, and night marine air temperature since the late nineteenth century. *Journal of Geophysical Research*, 108(D14), 4407. https://doi.org/10.1029/2002jd002670
- Ren, X., & Liu, W. (2021). The role of a weakened Atlantic meridional overturning circulation in modulating marine heatwaves in a warming climate. Geophysical Research Letters, 48(23), e2021GL095941. https://doi.org/10.1029/2021gl095941
- Seager, R., Blumenthal, M. B., & Kushnir, Y. (1995). An advective atmospheric mixed layer model for ocean modeling purposes: Global simulation of surface heat fluxes. *Journal of Climate*. 8(8), 1951–1964. https://doi.org/10.1175/1520-0442(1995)008<1951:aaamlm>2.0.co;2
- Simpson, I. R., Deser, C., McKinnon, K. A., & Barnes, E. A. (2018). Modeled and observed multidecadal variability in the North Atlantic jet stream and its connection to sea surface temperatures. *Journal of Climate*, 31(20), 8313–8338. https://doi.org/10.1175/jcli-d-18-0168.1
- Smeed, D. A., McCarthy, G. D., Cunningham, S. A., Frajka-Williams, E., Rayner, D., Johns, W. E., et al. (2014). Observed decline of the Atlantic meridional overturning circulation 2004–2012. Ocean Science, 10(1), 29–38. https://doi.org/10.5194/os-10-29-2014
- Soden, B. J., Held, I. M., Colman, R., Shell, K. M., Kiehl, J. T., & Shields, C. A. (2008). Quantifying climate feedbacks using radiative kernels. Journal of Climate, 21(14), 3504–3520. https://doi.org/10.1175/2007jcli2110.1
- Sévellec, F., Fedorov, A. V., & Liu, W. (2017). Arctic sea-ice decline weakens the Atlantic meridional overturning circulation. *Nature Climate Change*, 7(8), 604–610. https://doi.org/10.1038/nclimate3353
- Woollings, T., Gregory, J. M., Pinto, J. G., Reyers, M., & Brayshaw, D. J. (2012). Response of the North Atlantic storm track to climate change shaped by ocean–atmosphere coupling. *Nature Geoscience*, 5(5), 313–317. https://doi.org/10.1038/ngeo1438
- Xie, S. P., Deser, C., Vecchi, G. A., Ma, J., Teng, H., & Wittenberg, A. T. (2010). Global warming pattern formation: Sea surface temperature and rainfall. *Journal of Climate*. 23(4), 966–986. https://doi.org/10.1175/2009JCLI3329.1
- Zhang, R. (2008). Coherent surface-subsurface fingerprint of the Atlantic meridional overturning circulation. *Geophysical Research Letters*, 35(20), L20705, https://doi.org/10.1029/2008gl035463
- Zhang, R., Sutton, R., Danabasoglu, G., Kwon, Y., Marsh, R., Yeager, S. G., et al. (2019). A review of the role of the Atlantic meridional over-turning circulation in Atlantic multidecadal variability and associated climate impacts. Reviews of Geophysics, 57(2), 316–375. https://doi.org/10.1029/2019rg000644

HE ET AL. 11 of 11